JOUL, Volume *4*

Supplemental Information

Mechanically Stacked, Two-Terminal Graphene-Based Perovskite/Silicon Tandem Solar Cell with Efficiency over 26%

Enrico Lamanna, Fabio Matteocci, Emanuele Calabrò, Luca Serenelli, Enrico Salza, Luca Martini, Francesca Menchini, Massimo Izzi, Antonio Agresti, Sara Pescetelli, Sebastiano Bellani, Antonio Esaú Del Río Castillo, Francesco Bonaccorso, Mario Tucci, and Aldo Di Carlo

Supplemental Information

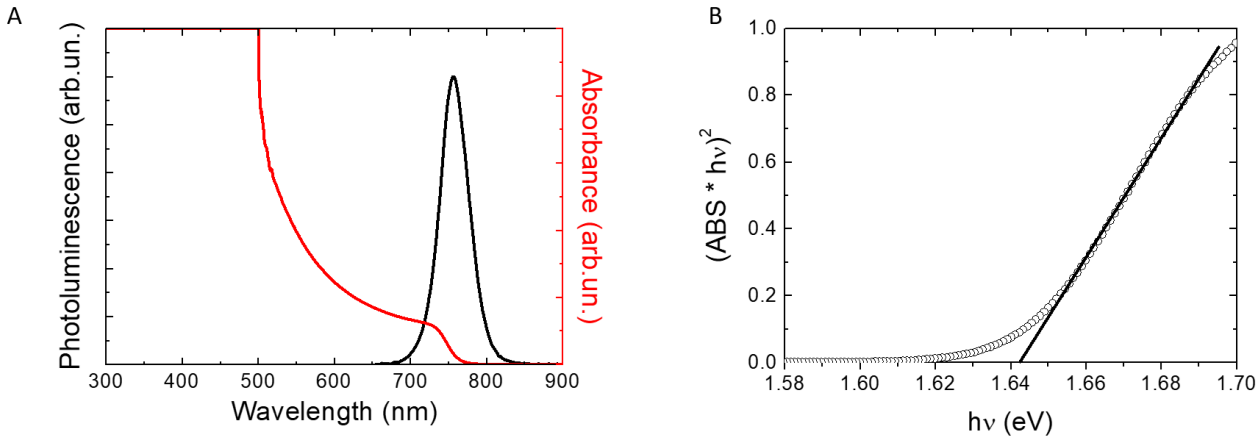

Figure S1 **(A)** Photoluminescence and absorbance of the perovskite absorber deposited over $cTiO_2/mTiO_2$ electron transport layer. **(B)** Tauc Plot analysis for optical bandgap estimation of the perovskite absorber.

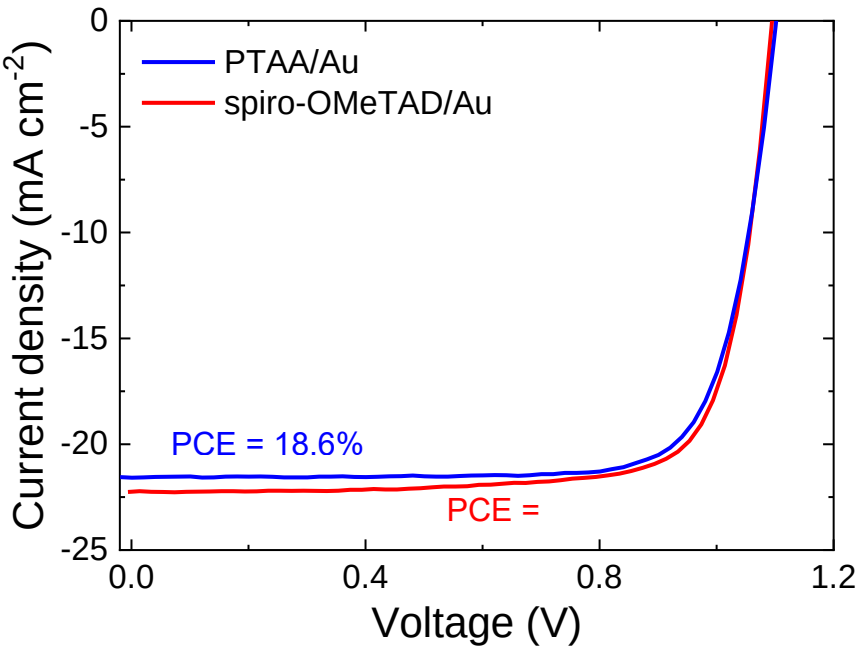

Figure S2 J-V characteristics of the reference mesoporous perovskite solar cells using spiro-OMeTAD (200 nm) or PTAA (40 nm) hole transporting layer and Au (80 nm) counter electrode. The J-V curves have been acquired in reverse voltage scan mode.

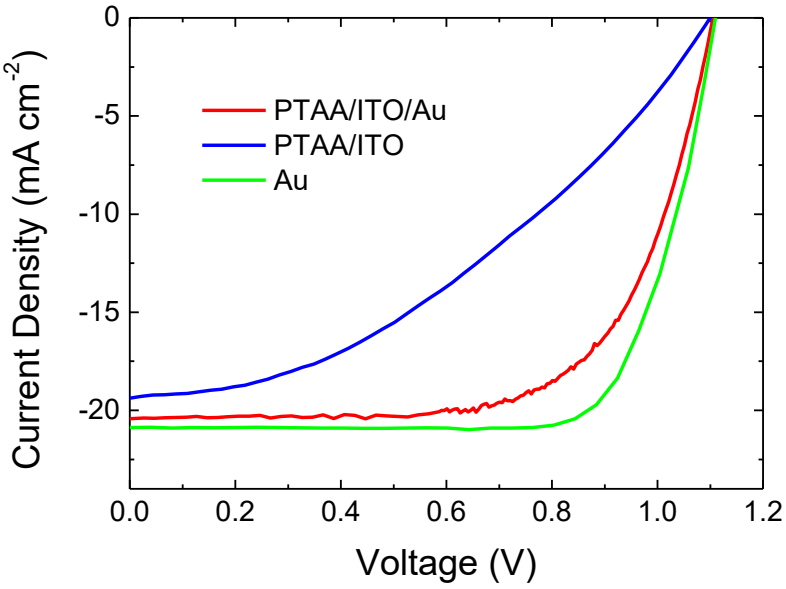

Figure S3 J-V characteristics of the same small area graphene-based perovskite solar cell using PTAA/ITO electrode before (blue curve) and after (red curve) Au deposition on ITO, compared against a cell from the same batch with the conventional Au electrode (green curve). The J-V curves have been acquired in reverse voltage scan mode.

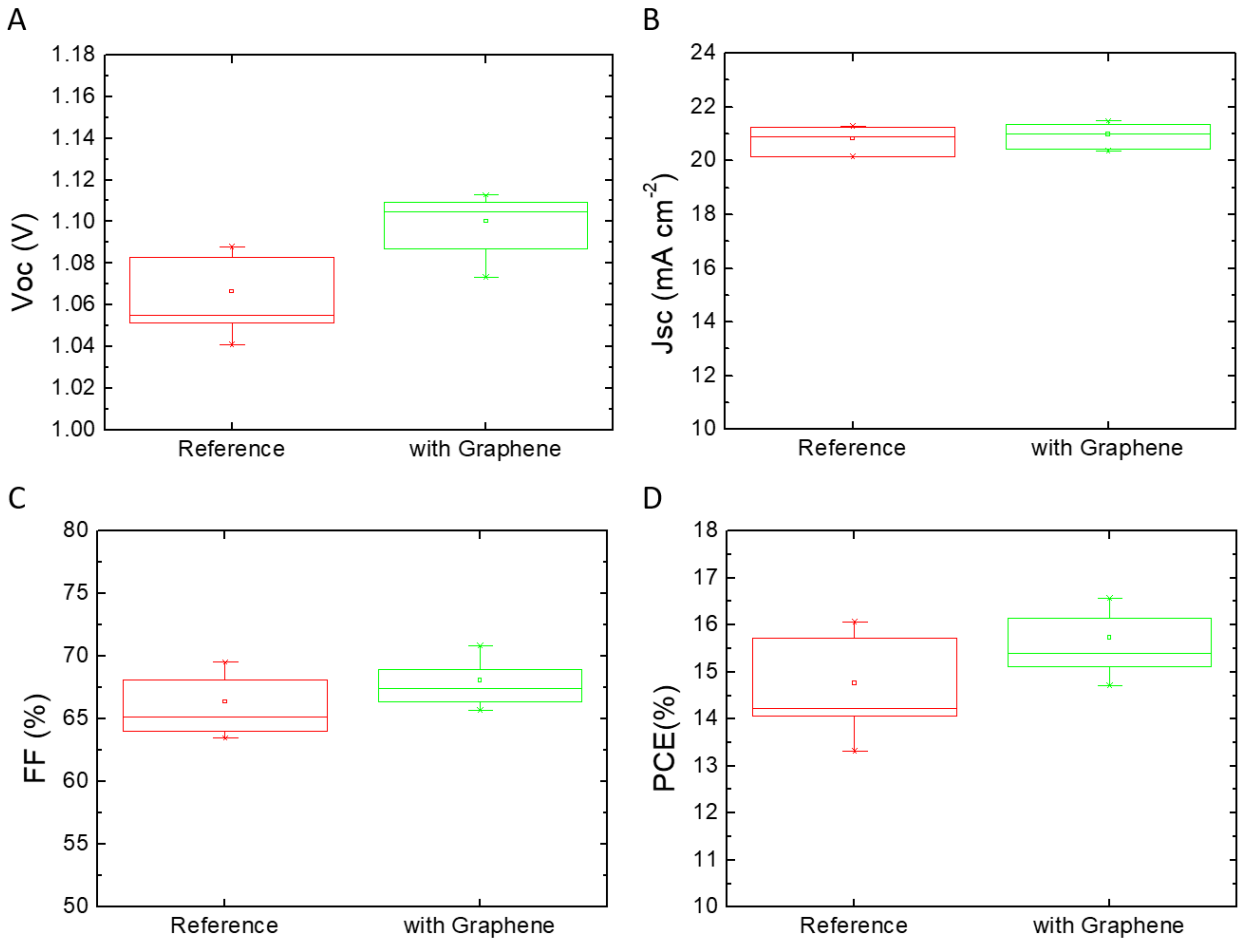

Figure S4 Statistical analysis of the Figures of Merit (FoM) of the small area perovskite solar cells with PTAA/ITO/Au counter electrode with and without graphene doping: **(A)** open-circuit voltage (Voc); **(B)** short-circuit current density (Jsc); **(C)** Fill Factor (FF); and **(D)** power conversion efficiency (PCE).

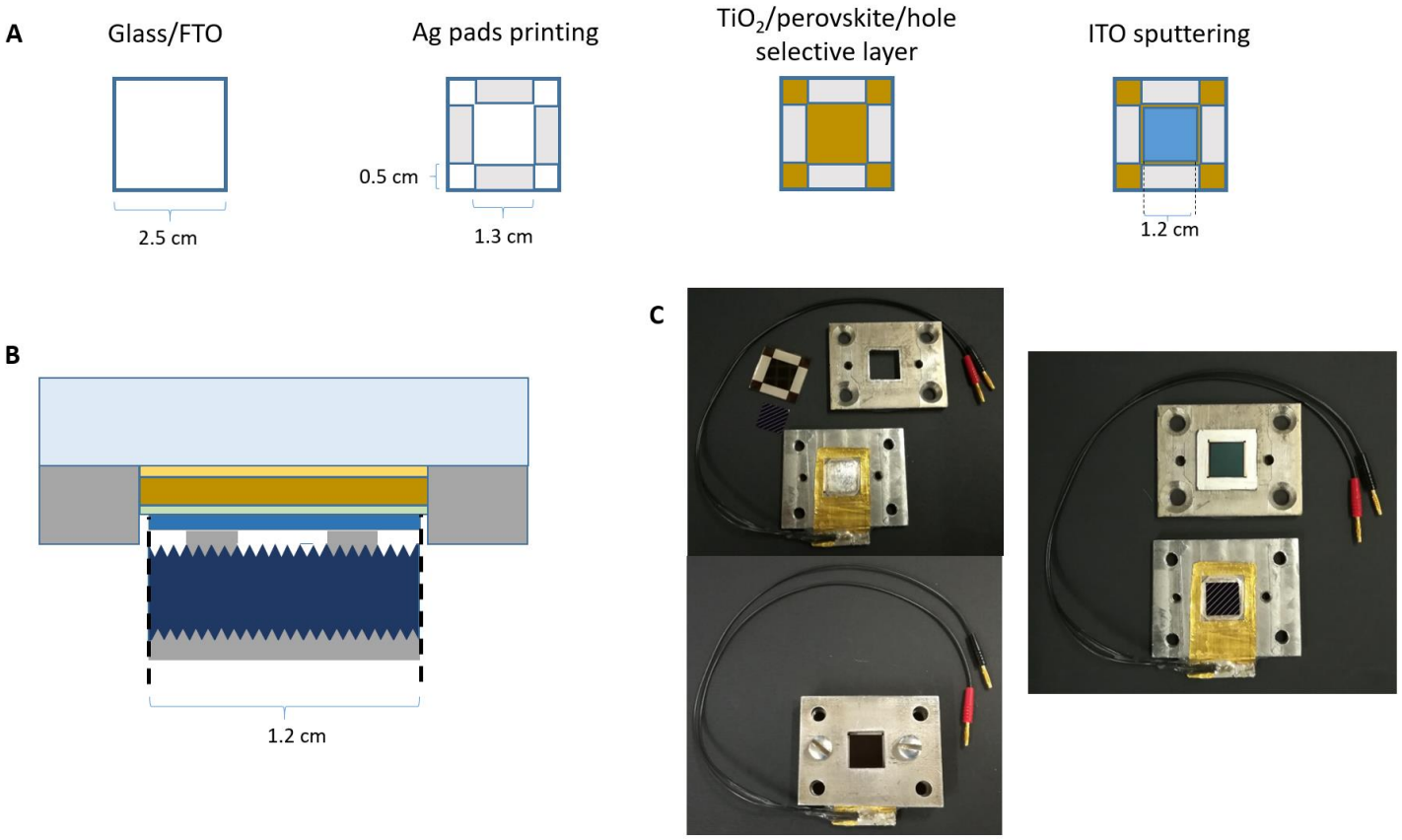

Figure S5 (A) sketch of the process flow of the perovskite solar cell, including the definition of the substrate, contacts and active area dimensions; **(B),** image of the coupled cells showing the direct contact between the fingers of the silicon bottom-cell and the ITO back electrode of the perovskite top-cell; **(C)** Photograph of the measurement set-up used to keep the sub-cells in contact.

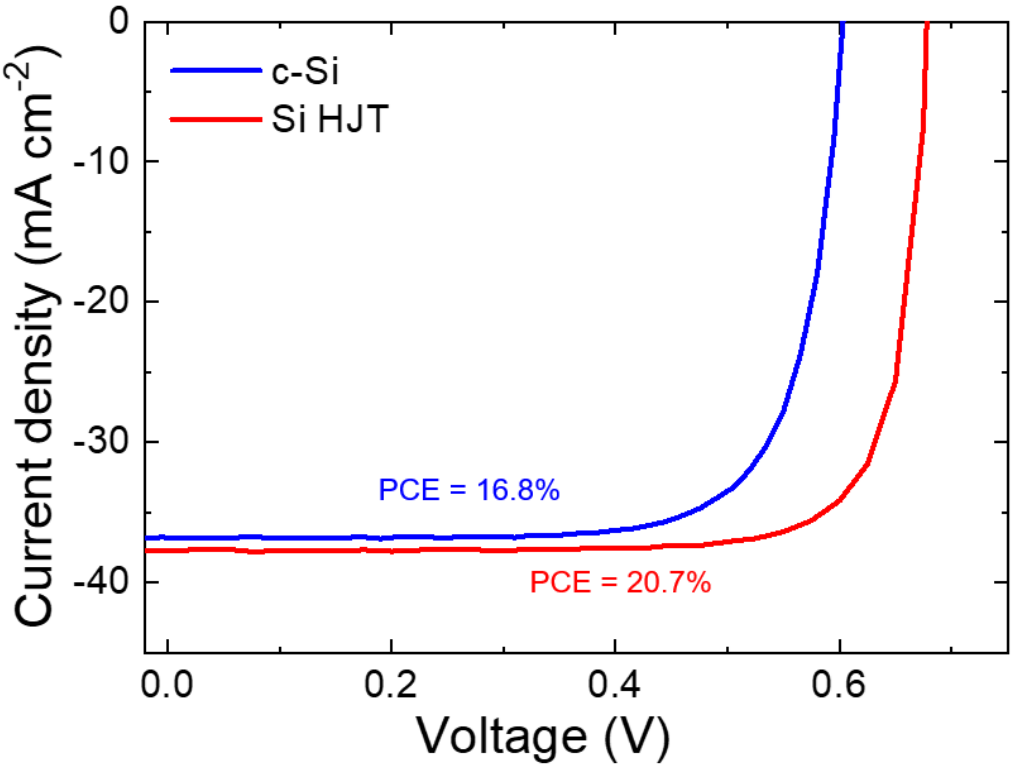

Figure S6 J-V characteristics measured for c-Si and Si HJT solar cells.

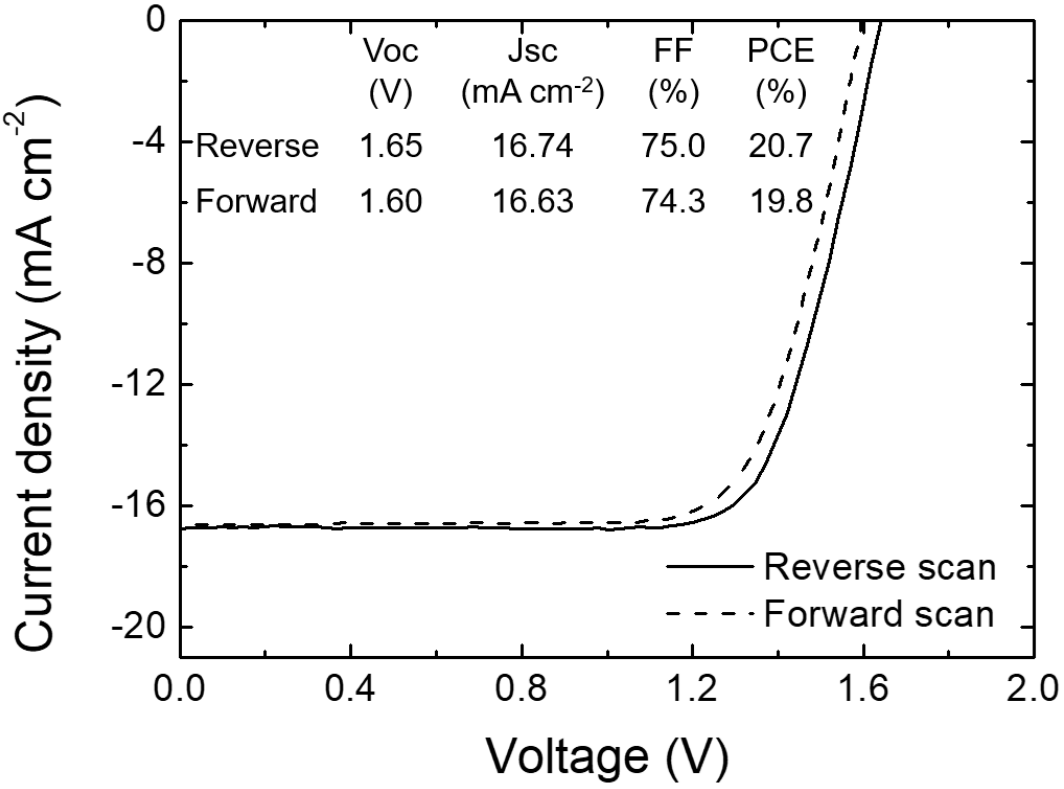

Figure S7 Forward and reverse J-V scan of a perovskite/c-Si mechanically stacked tandem, without graphene addition. The hysteresis behavior is the same observed for other devices based on this tandem architecture

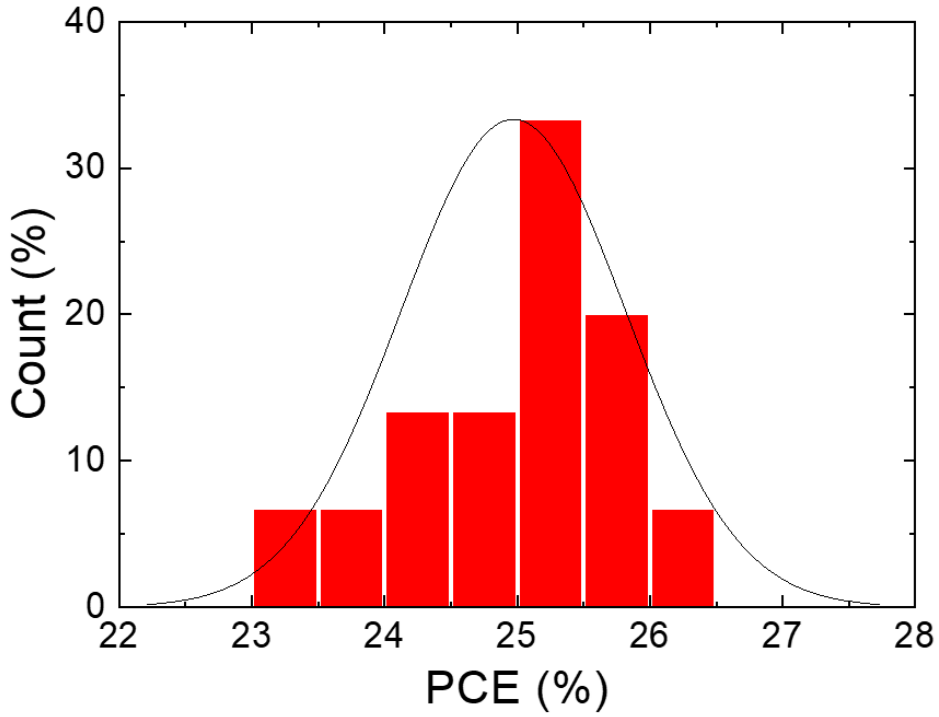

Figure S8 Statistical analysis of the PCE (estimated by J-V curves acquired in reverse voltage scan mode) measured on 15 graphene-based perovskite/Si HJT tandem obtained by mechanically stacking different graphene-based mesoscopic perovskite top-cells over the same Si HJT bottom-cell.

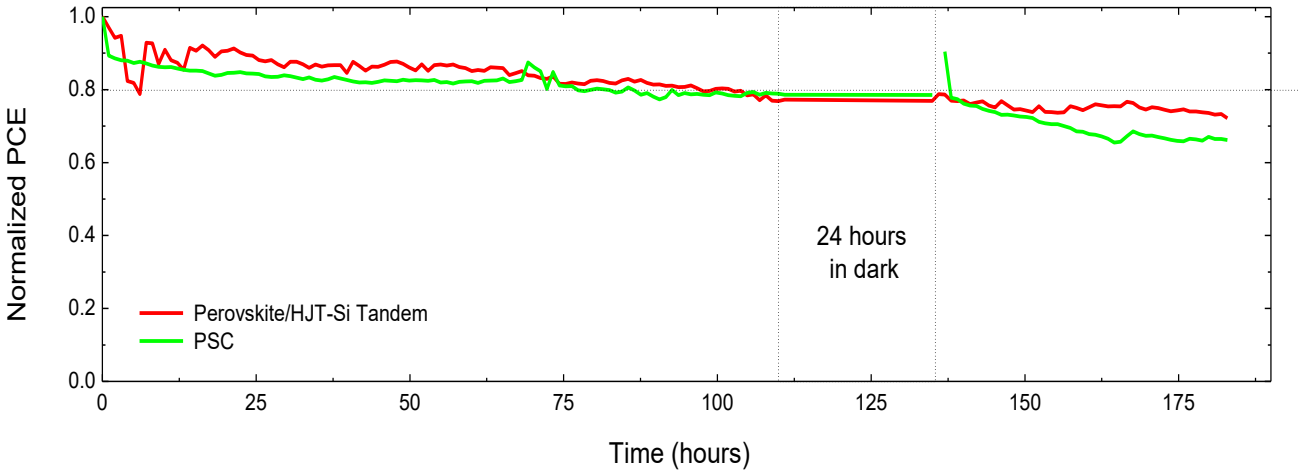

Figure S9 Stability of perovskite solar cell with ITO/Au electrode (green curve) and two-terminal mechanically stacked perovskite/silicon tandem (red curve) under continuous simulated 1 Sun illumination.

Table S1 Statistical analysis of the FoM (estimated by J-V curves acquired in reverse voltage scan mode) measured on 15 2-terminal mechanically stacked graphene based perovskite/Si HJT tandem devices.

Device	**V_{OC} (V)**	**J_{SC} (mA cm^{-2})**	**FF (%)**	**PCE (%)**
Perovkite/silicon HJT tandem	1.796 ± 0.008	17.955 ± 0.434	77.381 ± 0.856	24.970 ± 0.848